From structure to dynamics: Frequency tuning in the p53-Mdm2 network. II. Differential and stochastic approaches

Djomangan A. Ouattara, Wassim Abou-Jaoudé, Marcelle Kaufman

www.elsevier.com/locate/yjtbi

From structure to dynamics: Frequency tuning in the p53-Mdm2 network. II. Differential and stochastic approaches

Djomangan A. Ouattara, Wassim Abou-Jaoudé, Marcelle Kaufman

PII: S0022-5193(10)00164-5
DOI: doi:10.1016/j.jtbi.2010.03.031
Reference: YJTBI 5932

To appear in: *Journal of Theoretical Biology*

Received date: 9 October 2009
Revised date: 16 March 2010
Accepted date: 18 March 2010

Cite this article as: Djomangan A. Ouattara, Wassim Abou-Jaoudé and Marcelle Kaufman, From structure to dynamics: Frequency tuning in the p53-Mdm2 network. II. Differential and stochastic approaches, *Journal of Theoretical Biology*, doi:10.1016/j.jtbi.2010.03.031

From structure to dynamics: Frequency tuning in the p53-Mdm2 network. II. Differential and stochastic approaches.

Djomangan A. Ouattara, Wassim Abou-Jaoudé, Marcelle Kaufman*

Université Libre de Bruxelles (U.L.B.), Faculté des Sciences, Unit of Theoretical and Computational Biology, Campus Plaine C.P. 231, B-1050 Brussels, Belgium

***Corresponding author:**

Marcelle Kaufman

Université Libre de Bruxelles (U.L.B.), Faculté des Sciences,

Unit of Theoretical and Computational Biology,

Campus Plaine C.P. 231, B-1050 Brussels, Belgium

E-mail: Marcelle.Kaufman@ulb.ac.be

Tel.: +32 2 650 57 73

Fax: +32 2 650 57 67

Abstract

In Part I of this work, we carried out a logical analysis of a simple model describing the interplay between protein p53, its main negative regulator Mdm2 and DNA damage, and briefly discussed the corresponding differential model (Abou-Jaoudé et al., 2009). This analysis allowed us to reproduce several qualitative features of the kinetics of the p53 response to damage and provided an interpretation of the short and long characteristic periods of oscillation reported by Geva-Zatorsky et al. (2006) depending on the irradiation dose. Starting from this analysis, we focus here on more quantitative aspects of the dynamics of our network and combine the differential description of our system with stochastic simulations which take molecular fluctuations into account. We find that the amplitude of the p53 and Mdm2 oscillations is highly variable (to a degree that depends, however, on the bifurcation properties of the system). In contrast, peak width and timing remain more regular, consistent with the experimental data. Our simulations also show that noise can induce repeated pulses of p53 and Mdm2 that, at low damage, resemble the slow irregular fluctuations observed experimentally. Adding the stochastic dimension in our modeling further allowed us to account for an increase of the fraction of cells oscillating with a high frequency when the irradiation dose increases, as observed by Geva-Zatorsky et al. (2006).

Key-words

p53/Mdm2, feedback circuits, mathematical modelling, stochastic simulations, bifurcation analysis, oscillations.

1. Introduction

p53 is a key tumor suppressor protein that plays a major role in the control of the proliferation of genetically unstable cells (Ventura et al., 2007). It acts mainly as a transcriptional regulator and has been shown to be involved in a wide range of processes including cell cycle arrest, DNA repair, apoptosis and cellular senescence (Gatz and Wiesmüller, 2006; Oren, 2003; Vogelstein et al., 2000; Vousden and Lane, 2007). p53 also promotes the synthesis of its main antagonist, the ubiquitin ligase Mdm2, which negatively regulates p53 by accelerating its degradation (Brooks and Gu, 2006; Inoue et al., 2001). This negative feedback circuit between p53 and Mdm2 allows maintaining p53 at a low level in normal conditions. However, when cells are stressed or damaged, this homeostasis is disrupted, the level and activity of p53 increases leading to growth arrest, DNA repair or synthesis of pro-apoptotic proteins. Several experimental studies have shown that p53 and Mdm2 can exhibit oscillations after DNA damage caused by ionizing radiation (Bar-Or et al., 2000; Geva-Zatorsky et al., 2006; Hamstra et al., 2006; Lahav et al., 2004). At the level of cell populations, these oscillations have been observed to be damped (Bar-Or et al., 2000; Hamstra et al., 2006; Ramalingam et al., 2007), while single cell assays showed undamped oscillations over several hours after irradiation (Geva-Zatorsky et al., 2006; Lahav et al., 2004). In these studies on individual breast cancer cells (MCF7), the observation time was initially limited to 16 h following gamma irradiation (Lahav et al., 2004). The oscillations were reported to have a rather constant amplitude and a regular periodicity of about 7 h, the number of peaks increasing with the irradiation dose. Further investigations performed on a large number of individual cells and a time period of about 3 days after gamma irradiation, revealed much noisier oscillations and a large intercellular variability in response to radiation damage (Geva-Zatorsky et al., 2006). The oscillations were characterized by a rather regular periodicity and peak width but highly variable peak amplitudes. Following high irradiation doses (10 Gy gamma irradiation), 60% of the cells displayed oscillations with a characteristic period of about 5.5 h, whereas a significant fraction of irradiated cells showed either no

response or slowly-varying fluctuations. The oscillation period was shown to be a decreasing function of the irradiation dose, with a period of about 10 h at low irradiation doses and about 5.5 h at high irradiation doses. Moreover, a few cells changed frequency after 1 to 2 days of oscillation.

Several theoretical models have been proposed to reproduce and explain the oscillatory p53 and Mdm2 responses, in particular at the level of individual cells. Most of these theoretical studies used a deterministic approach based on ordinary differential equations (see e.g., Batchelor et al., 2008; Bottani and Grammaticos, 2007; Ciliberto et al., 2005; Ma et al., 2005; Wagner et al., 2005; Zhang et al., 2007) and only a few of them (Geva-Zatorsky et al., 2006; Proctor and Gray, 2008; Puszyǹski et al., 2008) focused on stochastic aspects of the dynamics. In Geva-Zatorsky et al. (2006), by introducing stochastic fluctuations in the protein production terms, the authors showed in particular that when the noise frequency is low, some of their simple models of the p53-Mdm2 loop can reproduce the variability in the amplitude of the p53 and Mdm2 oscillations observed experimentally. Taking stochastic effects into account at the level of transcriptional regulation and damage induction and repair, Puszyǹski et al. (2008) were able to reproduce oscillations of irregular amplitudes and well defined period as well as slowly-varying fluctuations prior to irradiation, as observed by Geva-Zatorsky et al. (2006). Finally, Proctor and Gray (2008) analyzed two stochastic models of the p53-Mdm2 network considering that Mdm2 was destabilized either by the $p14^{ARF}$ protein or by the ATM kinase. They predicted more regular oscillations in the presence of ARF than in the ATM model and proposed that this result might explain why Geva-Zatorsky et al. (2006) observed rather irregular oscillation in MCF7 cells that lack this protein.

However, in these last studies, there is no detailed analysis of the bifurcation properties of the models and on how these properties can influence the sensitivity to stochastic fluctuations. Moreover, some experimental observations, such as the increase of the fraction of cells oscillating with a high frequency when the irradiation dose increases, still remain to be

explained.

In a previous paper about the p53-Mdm2 system (Abou-Jaoudé et al., 2009), we have investigated the dynamical properties of a simple four-variable model derived from the work of Ciliberto et al. (2005) and centered on the role of Mdm2 in regulating the p53 response to DNA damage (Fig. 1). Combining a logical analysis with a differential approach, we have shown that the essential dynamical properties of our network are described by a small number of bifurcation scenarios that can be interpreted in terms of the balance between the positive and negative circuits of the network. These bifurcation scenarios depend on two parameters that can be linked to post-translational modifications of p53 and related to the DNA-binding affinity and transcriptional activity of p53, which are cell and stress type specific. This analysis qualitatively reproduces important features of the kinetics of the p53 response upon irradiation such as p53 pulses, failure to respond to damage, changes in the frequency of the oscillations in the course of the response or rapid dampening of the oscillations in a cell population. It also provides an interpretation of the high and low frequency oscillations observed by Geva-Zatorsky et al. (2006) depending on the irradiation dose in terms of two oscillatory regimes of significantly different periods as a function of the damage level.

In this paper we present a detailed analysis of the bifurcation properties of our differential model coupled with an analysis of the influence of molecular fluctuations on the dynamics of our system. We show that (1) the amplitude of the oscillations of p53 and Mdm2 is highly variable whereas peak width and timing are less affected by noise, (2) the degree of variability depends on the bifurcation properties of the system, (3) noise can induce repeated pulses of p53 and Mdm2 that, at low damage levels, may account for the slowly-varying fluctuations observed experimentally and (4) our model accounts for the increase of the fraction of cells showing high frequency oscillations when the irradiation dose increases.

2. Formulation of the model

As in Abou-Jaoudé et al. (2009), we consider the four-variable model shown in Fig. 1 and described by the following differential equations:

$$\begin{aligned}
\frac{\mathrm{d}[P]}{\mathrm{d}t} &= k_P \frac{K_P^4}{K_P^4 + [Mn]^4} - (d_P + d'_P[Mn])\,[P] \\
\frac{\mathrm{d}[Mc]}{\mathrm{d}t} &= k_{Mc} + k'_{Mc}\frac{[P]^4}{K_{Mc}^4 + [P]^4} - \left(k_{in} - k'_{in}\frac{[P]^4}{K_{Mn}^4 + [P]^4}\right)[Mc] \\
&\quad + \frac{1}{V_r}k_{out}[Mn] - d_{Mc}[Mc] \\
\frac{\mathrm{d}[Mn]}{\mathrm{d}t} &= V_r\left(k_{in} - k'_{in}\frac{[P]^4}{K_{Mn}^4 + [P]^4}\right)[Mc] - k_{out}[Mn] - d_{Mn}[Mn] \\
\frac{\mathrm{d}Dam}{\mathrm{d}t} &= k_{\mathrm{IR}} \cdot \mathrm{IR} - k_{Dam}\frac{[P]^4}{K_{Dam}^4 + [P]^4}Dam
\end{aligned} \tag{1}$$

where $d_{Mn} = d'_{Mn} + d''_{Mn}Dam/(K'_{Mn} + Dam)$. $[P]$, $[Mc]$, $[Mn]$ denote the concentrations of p53, cytoplasmic Mdm2 and nuclear Mdm2, respectively. Dam represents the level of DNA damage and IR the irradiation dose. A typical set of parameter values based on the literature (Ma et al., 2005; Oren et al., 1981; Reich et al., 1983; Pahl and Baeuerle, 1996) is given in Table 1[1].

The biological data underlying these equations can be summarized as follows. Nuclear Mdm2 down regulates active p53 by accelerating its degradation through ubiquitination (Brooks and Gu, 2006; Fang et al., 2000; Inoue et al., 2001) and by blocking its functional activity (Chen et al., 1995; Kruse and Gu, 2009; Oliner et al., 1993). The level of nuclear Mdm2 is itself up regulated by transport of cytoplasmic Mdm2 into the nucleus, which requires phosphorylation by the Akt kinase (Mayo and Donner, 2001; Zhou et al., 2001). Protein p53 both increases the synthesis of Mdm2 by transcriptional activation of gene *MDM2* (Barak et al., 1993; Freedman et al., 1999) and inhibits the nuclear entry of Mdm2. This negative control involves the inactivation of Akt through several PTEN-dependent

[1] In Abou-Jaoudé et al. (2009) the equations describing the interaction diagram in Fig. 1 are normalized so that some normalized threshold parameters take the value one.

(Feng et al., 2007; Gottlieb et al., 2002; Stambolic et al., 2001) as well as PTEN-independent pathways (Singh et al., 2002; Feng et al., 2007). The contribution of these different pathways depends on the cell type and stress intensity (Feng et al., 2007; Mayo et al., 2005). DNA damage is induced by transient exposure to stress and enables the accumulation of p53 by accelerating the degradation of nuclear Mdm2 through ATM-mediated phosphorylation and auto-ubiquitination (Bakkenist and Kastan, 2003; Stommel and Wahl, 2005). Finally, p53 also promotes DNA damage repair by inducing the synthesis of repair proteins (Adimoolam and Ford, 2003; Gatz and Wiesmüller, 2006; Lozano and Elledge, 2000; Offer et al., 1999).

The above nonlinear differential equations aim to provide a compact description of these multiple processes. Following the logical analysis in Abou-Jaoudé et al. (2009), we have introduced a nonlinear down regulation of the production of active p53 by nuclear Mdm2 to account for degradation-independent regulation of p53 function. This assumption may not be fully justified on biological grounds. However, as shown in Appendix, removing this term and using a nonlinear, Goldbeter-Koshland function (Goldbeter and Koshland, 1981) for the Mdm2-mediated degradation of p53 (Zhang et al., 2007) leads to qualitative similar behaviors (Fig. A1). Since it is well established that the transcriptional activity of p53 is strongly increased when p53 binds to DNA under the form of a tetramer (Chène, 2001; McLure and Lee, 1998; Weinberg et al., 2004) we use Hill functions with exponent $n = 4$ to describe the steps involving p53 transcriptional activity. Moreover, since DNA damage accelerates Mdm2 degradation through ATM-mediated phosphorylation, we also model this process by a nonlinear term.

To analyze the effect of molecular fluctuations on the dynamics of our system, we have transposed our differential model into a set of ten coupled reaction channels given in Table 2. The stochastic simulations are performed with the Gillespie's stochastic simulation algorithm (SSA) (Gibson and Bruck, 2001; Gillespie, 1977). This method of the Monte-Carlo type is widely used to study the effect of molecular noise on the dynamics of biochemi-

cal and genetic systems (see e.g., Andrecut et al. (2008); Dupont et al. (2008); Gonze et al. (2002a,b); Kummer et al. (2005)). It associates with each reaction channel i a probability p_i that depends on the specific reaction rate and is calculated from the reaction propensity w_i given in Table 2 according to the expression $p_i = w_i / \sum_i w_i$. At each time step, the algorithm randomly determines the next reaction that will occur according to its relative probability and the time interval for this reaction to take place. A scaling parameter denoted Ω permits the modulation of the number of molecules present in the system and thus the importance of internal fluctuations. At high values of Ω, the stochastic behavior of the system tends to the deterministic behavior governed by the differential model (1).

In the absence of precise data concerning the elementary steps, we still kept phenomenological rate laws in our stochastic model. Several authors have investigated the validity of the use of such rate laws in conjunction with the Gillespie's SSA. Their approaches rely on the separation of timescales that often occur in biochemical systems. Rao and Arkin (2003), by separating slow and fast species, show that Michaelis-Menten rate laws may be derived in a stochastic formulation using scaling arguments and quasi-steady-state assumptions (QSSA). Moreover, they suggest that stochastic analogs of Hill functions may also apply provided they are well justified in the deterministic case. More generally, several multi-scale methods have recently been proposed with the purpose of reducing the complexity and speeding up stochastic simulations of protein interaction networks, while maintaining a good accuracy (Goutsias, 2005; Barik et al., 2008; Macnamara et al., 2008). In particular, Barik et al. (2008) have extended the work of Rao and Arkin (2003) by introducing the total quasi-steady-state assumption that allows removing the limitations of the classical QSSA (Ciliberto et al., 2007). Their method remains accurate even in conditions of poor time scale separation. See also Macnamara et al. (2008). Considering Michaelis-Menten-type rate expressions and Hill functions in our stochastic simulations implies assumptions about relative concentrations and time-scales that are subject to the same restrictions as in the deterministic framework. However the advantage of this simplified stochastic approach is

to importantly reduce the number of interactions and variables, as well as the number of adjustable parameters.

3. Bifurcation analysis and stochastic simulations

The core of the network is described by the first three differential equations of system (1). We have analysed its bifurcation properties as a function of two key parameters whose importance for the dynamical properties of the system has been emphasized in our previous logical analysis (Abou-Jaoudé et al., 2009): the degradation rate of nuclear Mdm2 (d_{Mn}), which reflects the level of DNA damage, and the ratio K_{Mc}/K_{Mn}, which is related to the binding affinity of p53 for its target genes and influences the balance between the positive and negative feedback loops of the core network. In Abou-Jaoudé et al. (2009), we have shown that parameter k'_{in} also plays an important role for this balance. Here, we consider a value of k'_{in} such that oscillatory responses prevail for a large domain of d_{Mn} values.

Varying K_{Mc} while keeping K_{Mn} constant (or vice-versa, see Fig. S1, supplementary material), allows one to define three main domains characterized by different bifurcation scenarios that could be associated with cell- and stress-type specific differences. A typical example of the sequence of bifurcations for each one of these three domains is shown in Fig. 2, for increasing values of K_{Mc}, and discussed below. For each bifurcation scenario, the dynamical behavior upon irradiation is illustrated by stochastic simulations.

3.1. First bifurcation scenario: low values of K_{Mc} or high values of K_{Mn}

For low K_{Mc} (or high K_{Mn}) values, when the degradation rate of nuclear Mdm2 (d_{Mn}) increases (*i.e.* when the level of damage increases), the system displays successively a stable steady state with a low level of p53, an oscillatory regime and a stable steady state where the level of p53 remains higher than in the rest state at low d_{Mn} (Fig. 2(a)). At low d_{Mn}, the oscillations arise with small amplitude from a supercritical Hopf bifurcation while at high d_{Mn}, they emerge with large amplitude from a subcritical Hopf bifurcation under the

influence of the positive feedback circuit of the core network. The oscillation period is rather constant over a wide range of the oscillatory domain and the mean level of p53 remains low. Fig. 3(a) shows a typical stochastic simulation of the response of the system upon damage induction. Before irradiation, the system is in its rest state with a low level of p53 and high level of Mdm2. Upon damage induction, large amplitude oscillations of p53 and Mdm2 appear, each p53 pulse leading to the repair of a certain amount of damage. A Fourier analysis on a cell population shows that, on average, these oscillations have a characteristic period of about 8.5 h (Fig. 3(b)). When most damage has been repaired, one can observe slowly-varying irregular fluctuations of p53 and Mdm2. Finally, when all the damage has disappeared, the system settles back in its rest state.

In this situation where the binding affinity of p53 for gene $MDM2$ is considered to be stronger than its binding affinity for the genes that are involved in the downregulation of the translocation of Mdm2 into the nucleus, the negative feedback circuit of the core network prevails over the positive circuit and, from a structural point of view, this case is rather close to the one described in the models of (Chickarmane et al., 2005; Ma et al., 2005; Wagner et al., 2005).

3.2. Second bifurcation scenario: high values of K_{Mc} or low values of K_{Mn}

For high values of K_{Mc} (or low values of K_{Mn}) as in Fig. 2(c), the bifurcation scenario differs from the previous case by the sequence in which the feedback circuits generate their characteristic dynamics as d_{Mn} increases. At low d_{Mn} values, it is now the positive feedback loop that becomes active in the first place. As d_{Mn} increases, the system displays successively a stable rest state with a low level of p53, the coexistence of this stable steady state with a second stable state or an oscillatory state, a stable oscillatory regime and finally again a single steady state but now with a high level of p53. Here, the oscillations arise from supercritical Hopf bifurcation points on the upper branch of an S-shaped steady state curve. The existence of a multistationarity domain at low d_{Mn} ensures the onset of oscillations of

significant amplitude when damage is induced. The oscillations are characterized by a short period, smaller peak amplitudes and high average value of p53. Fig. 4(a) shows two typical stochastic simulations upon damage induction starting from the rest state. As discussed in section 4, these oscillations are much more variable than in the case of the preceding bifurcation scenario. A Fourier analysis on a cell population shows that, on average, they have a characteristic period of about 5.5 h (Fig. 4(b)). Moreover, one observes that, before returning to the rest state, some cells may continue temporarily to oscillate after damage repair. A similar behaviour has been observed in Toettcher et al. (2009). This situation can here be explained by the presence, in the deterministic limit, of a region of coexistence of the rest state with the oscillatory state or stable node-focus (Fig. 2(c)). However, molecular fluctuations drive the system sooner or later back to the rest state.

At higher values of the ratio K_{Mc}/K_{Mn}, the limit cycle oscillations disappear and the steady states on the upper branch of the sigmoidal curve become stable node-foci. In the stochastic description, however, in the presence of damage, small fluctuations may be amplified and give rise to repeated pulses of p53 and Mdm2 until damage is fully repaired (result not shown; see also section 6).

3.3. Third bifurcation scenario: intermediate values of K_{Mc} and K_{Mn}

For intermediate values of K_{Mc} and K_{Mn} (Fig. 2(b)), the general picture remains similar to the preceding bifurcation scenarios with, as d_{Mn} increases, a stable rest state with a low level of p53 followed successively by an oscillatory domain and a stable steady state with a high level of p53. Here, however, an important feature is now the existence, as a function of d_{Mn}, of two oscillatory regimes of significantly different periods, amplitudes and mean levels, separated by a cyclic fold. Large amplitude oscillations, at low d_{Mn}, are generated from an infinite-period bifurcation. They are characterized by a low frequency and low average value of p53. At high d_{Mn}, the oscillations arise from a supercritical Hopf bifurcation and are characterized by smaller amplitudes, a high frequency and higher mean

level of p53. Interestingly, the ratio of the periods of the two oscillatory regimes is close to two as in the experiments of Geva-Zatorsky et al. (2006) (see Figure S3 of this reference).

As reported in Abou-Jaoudé et al. (2009), this bi-cyclicity renders the system very sensitive to the level of damage and efficiency of damage repair (k_{Dam}), which is illustrated here by the stochastic simulations in Fig. 5.

Fig. 5(a) and (b) correspond to situations where the cells are stressed with a high radiation dose. When the rate of damage repair is low (Fig. 5(a)), as long as the level of damage remains high, the system presents oscillations of high frequency and mean level, corresponding to Region I in Fig. 2(b). The characteristic period of these oscillations is about 4.5 h. Note that in the stable node-focus region at high damage level, the oscillations are driven by the molecular noise. This feature is discussed in Section 6. As damage is being progressively repaired, the system reaches the bi-cyclic region (Region II in Fig. 2(b)) where it oscillates randomly between the two coexisting oscillatory regimes, with a characteristic period of about 8 h. When the level of damage becomes low, the system shifts to Region III characterized by large amplitude oscillations of low mean level and a period of about 8.5 h. When the rate of damage repair is high (Fig. 5(b)), there are no frequency shifts. After irradiation, the system passes quickly through Regions I and II and displays only large amplitude oscillations of low frequency with a characteristic period of about 10 h. For low damage levels (Fig. 5(c)), the system also exhibits large amplitude oscillations of low frequency, corresponding to Region III in Fig. 2(b), independently of the repair rate. These results suggest that different cells in a same population could behave differently according to their damage level or repair efficiency and provide an interpretation of the experimental observation that some irradiated cells change frequency after 1–2 days of oscillation (Geva-Zatorsky et al., 2006).

Importantly, stochastic simulations on cell populations also show that the fraction of cells oscillating with a high frequency increases with the irradiation dose (Fig. 6), in good qualitative agreement with experimental data (Geva-Zatorsky et al., 2006, Figures 3 and S3).

Since damage is induced stochastically in our simulations, different cells acquire different levels of damage, the fraction of cells that oscillate increasing rapidly with the irradiation dose. At low irradiation doses, most cells are characterized by a period of about 10 h with a shift towards a period of about 5 h when the irradiation doses are increased. Note that in the experimental data, some cells show an oscillating behavior in the absence of irradiation (Fig. 6(b), *top*) with a broad distribution of periods. This is not reproduced in our simulations since our basal d_{Mn} value has been chosen such that there are no noise-induced pulses or oscillations prior to damage induction[2]. However, the level of damage has not been measured in the experiments of Geva-Zatorsky et al. (2006) and it is possible that some cells are already damaged before irradiation. This could result from sources of damage other than irradiation that are not considered in our mathematical model.

It should also be noted that for the bifurcation scenarios corresponding to lower and higher K_{Mc} values (here, $K_{Mc} = 0.15$ and 1.3 nM), such an increase in the frequency with the irradiation dose is not observed. This suggests that an appropriate ratio K_{Mc}/K_{Mn} and thus an appropriate balance between the positive and negative feedback loops of the network, leading to the existence of two distinct oscillatory regimes (as is the case here for $K_{Mc} = 0.6$ nM), may be required for the emergence of this behavior. An alternative explanation for an increase in frequency with the irradiation dose could be a change of bifurcation scenario depending on the stress intensity and the post-translational modifications (Mayo et al., 2005) that may modify the binding affinities of p53 (here, the values of K_{Mc} and K_{Mn}). This alternative would correspond to a shift from low K_{Mc}/K_{Mn} values (low frequency) to high K_{Mc}/K_{Mn} values (high frequency) as the irradiation dose increases.

In the next section, we quantify the variability of the oscillations for the different situations presented here and show that this variability depends on the bifurcation properties of the system.

[2]Somewhat higher basal values of d_{Mn} lead to slow irregular pulses in the absence of irradiation, as discussed in section 6.

4. Oscillation variability is bifurcation specific

The concentration levels of p53 in mammalian cells that are reported in the literature vary from nano to micromolar ranges (Hu et al., 2007; Hsu et al., 2004; Ma et al., 2005). Here, we have analysed the dynamics of p53 and Mdm2 for concentration levels in the nanomolar range, corresponding to values of Ω that vary from 1 to 50. For higher values of Ω, the level of noise is low in our system and the stochastic dynamics becomes close to the deterministic one. We have also assumed that the nuclear concentration of Mdm2 is in the same range as the nuclear concentration of p53. To quantify the effect of stochastic fluctuations on the behavior of the system, we have used the peak amplitude and width variability as defined in Geva-Zatorsky et al. (2006), as well as the autocorrelation function for the timing of the peaks. The computational procedures are described in Section 1 of the supplementary material.

To assess the effect of molecular noise on the variability of the different oscillatory regimes avoiding the influence of other, noise-independent, factors such as damage repair or the vicinity of bifurcation points, we have first studied the oscillation variability at constant d_{Mn} values. We have analyzed the time course of the level of p53 and Mdm2 for 100 individual cells in the case of high and low frequency oscillations, respectively. Our simulations show that the oscillations of high frequency and small amplitude, which, in the deterministic limit, emerge from supercritical Hopf bifurcations, present more variable peak amplitudes and widths than the oscillations of low frequency and large amplitudes that arise through an infinite-period or subcritical Hopf bifurcation. Fig. 7(a) and (b) show two simulations performed at constant d_{Mn} values (i.e. without DNA damage repair) for $K_{Mc} = 0.15$ nM and $K_{Mc} = 1.3$ nM, respectively. After damage induction, the low frequency p53 oscillations have a variability of 25% for the peak amplitude and 10% for the peak width. For the high frequency oscillations, this variability is about 40% for the peak amplitude and 25% for the peak width. In both cases, the variability of the peak timing is comparable to that of the peak width (about 8% and 20%, respectively). In addition, the autocorrelation functions

for the time course of p53, while following each one of these two oscillatory regimes, give a correlation time of 43 hours for the low frequency oscillations versus 8 hours for the high frequency oscillations, confirming that the timing of the p53 peaks is much more affected by molecular fluctuations on the high frequency oscillatory regime. Note that this bifurcation-specificity of the influence of molecular fluctuations is independent of the level of Mdm2 and p53 proteins available in the system, i.e. the level of internal noise (Figs. S2 and S3, supplementary material).

For $K_{Mc} = 0.6$ nM, we have also analyzed the sensitivity of the system to noise in the region where, in the deterministic description, the low and high frequency limit cycles coexist. Our results show that the variability of the peak amplitude is further enhanced in this region due to the fact that the system oscillates randomly between the two limit cycles under the influence of the molecular fluctuations (see Fig. 7(c)). In this particular case, a statistical analysis gives a bimodal distribution in peak amplitude (representative of the two distinct amplitudes) with a variability of 50%, whereas peak width remains rather robust with a variability of 15%. A Fourier analysis shows a dominant period of about 8.5 h in this region, which is characteristic of the low frequency limit cycle. Note that when damage repair is taken into account in our simulations, the bimodal distribution of the peak amplitudes of p53 tends to disappear (see supplementary material, Fig. S5(b)).

Table 3 summarizes the variability of the amplitude and peak width of the oscillations of p53 and Mdm2 in our stochastic model for $\Omega = 1$ and a constant damage level.

5. Influence of damage repair and transient dynamics on the oscillation variability

As mentioned above, several additional factors, such as the damage repair, large transient p53 peaks before stabilization in the oscillatory regime and the neighbourhood of bifurcation points, may contribute to increase the variability of the oscillations. See Table 4 and supplementary material (Figs. S2, S3 and S4). One observes that the stochastic repair process

mainly increases the variability of the peak amplitude of the low frequency oscillations but has, in general, no significant effect on the high frequency oscillations. This can be expected from the bifurcation diagrams in Fig. 2(a) and (b), where the amplitude of the low frequency oscillations decreases monotonously when d_{Mn} decreases, while the amplitude of the high frequency oscillations (Fig. 2(c)) remains rather constant. In addition, during this repair process, the system passes through different bifurcation points that may influence the oscillation variability if the system stays for a long time in the vicinity of these bifurcation points, in particular infinite-period or saddle-node bifurcation points. This feature is discussed and illustrated in Section 4 of the supplementary material. Also of note, upon damage induction, the system presents a few large transient p53 and Mdm2 peaks before stabilizing in the oscillatory regime. These transients are characteristic of supercritical Hopf bifurcations and are mainly present on the small amplitude oscillatory regimes (or stable node-foci) where they significantly contribute in enhancing the variability of the peak amplitude (See, for example, Fig. S2(b) and (d)).

6. Noise can induce repeated pulses of p53 and Mdm2

In the framework of our model, one observes that noise can induce oscillations in regions where, in the deterministic regime, the steady states are stable node-foci or in regions where stable and unstable steady states coexist. Let us consider the case where $K_{Mc} = 0.6$ nM and $\Omega = 1$ (Fig. 8). At high damage level (high d_{Mn}), in the region of the stable node-focus, small fluctuations are amplified and lead to persistent p53 and Mdm2 oscillations with a characteristic period of about 5.3 h (Fig. 8(a)) and a rather high amplitude and width variability (Table 3, column 5). For decreasing noise levels (higher values of Ω), the amplitude of these noise-induced oscillations decreases but the period and variability do not change (not shown). In this case, random fluctuations continually cause the system to execute cyclic trajectories in the basin of attraction of the node-focus and the oscillation period is determined by the cycling properties of this node-focus. The average dynamics at

the level of cell populations corresponds to damped oscillations.

At low damage levels (low d_{Mn}), one observes that noise induces irregular p53 pulses in the multistationarity region where the rest state coexists with unstable steady states (Fig. 8(b)). Simulations on a population of 100 cells show that the number of pulses and the fraction of cells showing a pulsatile behavior increases when the distance from the stable steady state to the neighbouring unstable steady state decreases. Indeed, for $d_{Mn} = 0.55$ h^{-1}, only a few cells ($\sim 3\%$) show one or two transient peaks of p53. For $d_{Mn} = 0.6$ h^{-1} (resp. 0.65 h^{-1}), 75% (resp. 100%) of the cells display transient peaks, with some cells showing quasi-regular oscillations with a very long characteristic period of ~ 20 h (Fig. 8(b), cell 3). These p53 pulses have a large amplitude and rather low variability as for the low frequency limit cycle. The pulse timing depends on the noise characteristics (here, white noise) rather than on cycling properties of the system. This type of noise-induced pulses depends on the level of noise and is typical of stochastic resonance, as discussed in Tyson (2006). Contrary to the noise-induced oscillations at high damage (high d_{Mn}), the average dynamics at the level of cell populations does not resemble oscillations.

7. Discussion

Experimental studies of the kinetics of p53 have revealed a great intracellular and intercellular variability of the oscillatory response in irradiated cells. In order to reproduce and interpret these observations, we have studied a simple model of the p53-Mdm2 network that consists of an antagonist circuit between p53 and nuclear Mdm2 embedded in a three-element negative circuit between p53, nuclear and cytoplasmic Mdm2. To analyze the dynamical properties of this model, we have developed an integrated approach in which different levels of description complement each other and have combined a logical modeling method with a differential approach and stochastic simulations. The logical approach has allowed us to unveil the main dynamical potentialities of the network in terms of the balance between the positive and negative feedback circuits, to bring out the key role for the

dynamics of the system of parameters linked to the transactivational properties of p53, and to reproduce qualitatively several experimental observations, without necessitating detailed quantitative data (Abou-Jaoudé et al., 2009). The differential approach has permitted to refine the bifurcation analysis in the framework of a more realistic model and has provided more quantitative information on important aspects of the dynamics such as the period and the amplitude of the oscillations. Finally, the stochastic approach has enabled us to study the influence of molecular fluctuations on the behavior of the network, to reproduce the stochastic aspects of the dynamics of p53 observed experimentally and to draw the distribution of important characteristics of the oscillations in cell populations.

This combined analysis enabled us to bring out several interesting dynamical properties of our model and to reproduce various features of the experimental data that have not been addressed in other modeling approaches. It shows the existence of two oscillatory modes of significantly different periods, mean levels and amplitude depending on characteristics such as the affinity of p53 for its targets, the level of damage or the repair rate. As discussed in Abou-Jaoudé et al. (2009), this feature provides an interpretation for the short and long characteristic periods of oscillation reported by Geva-Zatorsky et al. (2006) depending on the irradiation dose, as well as for the changes in the oscillation frequency in the course of the response that have been observed for some cells several hours after irradiation. As shown here, it also allows to account for an increase in the fraction of cells oscillating with a high frequency when the irradiation dose increases.

The stochastic analysis of our model network further shows that the large amplitude limit cycle oscillations of low frequency, generated by infinite-period or subcritical Hopf bifurcations, are less sensitive to molecular fluctuations than the high frequency oscillations arising from supercritical Hopf bifurcations. In the spirit of Tyson (2006), we suggest that this bifurcation specificity might contribute to explain the difference between the highly variable oscillations (of period of about 5.5h) reported by Geva-Zatorsky et al. (2006) and the more regular pulses of lower frequency observed by Lahav et al. (2004). Finally, our

stochastic analysis shows the existence of noise-induced repetitive pulses of p53 and Mdm2 at high and low damage levels, where the deterministic description displays stable steady states. At high damage the characteristics of these noise-induced oscillations are close to those of the small amplitude oscillations arising in the limit cycle region (similar regular period, small amplitudes and a high average value of p53), but their amplitudes and peak width are more variable. On the contrary, slow transient pulses generated by stochastic resonance at very low damage have an irregular periodicity and weak variability. Such slow transient pulses have also been observed in Puszyǹski et al. (2008) and, as suggested by Tyson (2006), they may account for the slowly-varying fluctuations observed in a fraction of cells by Geva-Zatorsky et al. (2006).

Consistent with the experimental data, the p53 and Mdm2 oscillations in our stochastic simulations are characterized by noisy amplitudes but rather regular peak width and timing. However, the level of stochasticity in our model remains lower than in the experimental observations, as has also recently been observed for a detailed stochastic model of the p53-Mdm2/Mdmx circuit (Cai and Yuan, 2009). Moreover, the correlation between the amplitudes of the peaks of Mdm2 and p53 is much higher than the one reported for the experiments of Geva-Zatorsky et al. (2006). Estimations over 72h after damage irradiation show a correlation coefficient of 0.3 ± 0.5 for the large amplitude oscillations and 0.8 ± 0.3 for the small amplitude oscillations, compared to a correlation of 0 ± 0.2 in the experimental data. This discrepancy suggests that the sole interactions between p53 and Mdm2 modelled here are not sufficient for accurately describing the functioning of the p53-Mdm2 regulatory network and that additional interactions would importantly contribute to the p53 oscillatory response upon irradiation. Recently, Batchelor et al. (2008) proposed that p53 oscillations are externally driven by pulses in the upstream signalling kinases, ATM and Chk2. Such interactions may contribute to increase the level of stochasticity in the network and break the correlation between the amplitudes of the p53 and Mdm2 peaks.

If the existence of p53 oscillations (or pulses) is now well-established, their importance

and physiological function still remain to be clarified. Several possibilities have been put forward such as, for example, an increase of the range of possible dynamical behaviors of the target genes of p53 compared with constant p53 levels (Batchelor et al., 2009; Lahav, 2008). Our study suggests that the p53-Mdm2 network would be capable of tuning the shape, the frequency and mean level of the oscillations by generating different oscillatory patterns as a function of the severity of the damage. Therefore, we recently investigated, in the framework of a simple model, the role of the different oscillatory regimes found in this work on downstream genes involved in apoptosis. Our first results indicate that oscillations increase the activating strength of p53, as also illustrated by Wee et al. (2009) in the case of a simple example of a gene-protein interaction. Moreover, we observe that, at high damage, oscillations of high frequency and mean level tend to rapidly activate apoptosis. On the contrary, when the damage severity is low, the large amplitude oscillations characterized by a low duty cycle (large interspike interval), favor cell-cycle arrest and repair unless damage repair is too slow. These results suggest that the shape of the oscillations could play a role in the activation of pro-apoptotic genes.

Acknowledgements

We thank Didier Gonze for fruitful discussions. We acknowledge financial support from a EU STREP Grant (COMBIO) and the Communaut Franaise de Belgique (ARC Grant 04/09-307). W. A-J has been supported by grants from the Fonds pour la formation à la Recherche dans l'Industrie et l'Agriculture and the David and Alice Van Buuren Foundation. The bifurcation analysis has been performed with XPPAUT (http://www.math.pitt.edu/~bard/xpp/xpp.html).

Appendix

Alternative formulation of the model

Here we present an alternative formulation of our model of the p53-Mdm2 network where the down regulation of the production of active p53 by nuclear Mdm2 has been removed. Following Zhang et al. (2007) and Zhang et al. (2009), we also assume that nuclear Mdm2 accelerates the degradation of p53 when its concentration exceeds a certain threshold value and choose a Goldbeter-Koshland (GK) function to model this effect (Goldbeter and Koshland, 1981). In this case, the equation for the evolution of p53 becomes

$$\frac{\mathrm{d}[P]}{\mathrm{d}t} = k_P - d_P[P] - d'_P \cdot G([Mn], a, \frac{J_1}{[P]}, \frac{J_2}{[P]})[P] \tag{2}$$

with

$$G(u, v, q, r) = \frac{2u \cdot r}{v - u + v \cdot q + u \cdot r + \sqrt{(v - u + v \cdot q + u \cdot r)^2 - 4u \cdot r(v - u)}}$$

A bifurcation analysis of this model as a function of d_{Mn} and K_{Mc} has been performed. For appropriate parameter settings, this model exhibits the same bifurcation sequences as the initial model with the emergence of bicyclicity for intermediate values of K_{Mc} (compare Figs. A1 and 2). Note that when the GK function is replaced by a bilinear degradation term in equation (2), this bicyclic behavior is lost, indicating that a sufficient non-linearity in the down-regulation of active p53 by nuclear Mdm2, either at the level of the production of p53 (see model (1)) and/or at the level of its degradation, would be necessary for the emergence of this feature.

References

Abou-Jaoudé, W., Ouattara, D. A., Kaufman, M., Jun 2009. From structure to dynamics: frequency tuning in the p53-mdm2 network i. logical approach. J Theor Biol 258 (4), 561–577.

Adimoolam, S., Ford, J. M., Sep 2003. p53 and regulation of dna damage recognition during nucleotide excision repair. DNA Repair (Amst) 2 (9), 947–954.

Andrecut, M., Cloud, D., Kauffman, S. A., Feb 2008. Monte carlo simulation of a simple gene network yields new evolutionary insights. J Theor Biol 250 (3), 468–474.

Bakkenist, C. J., Kastan, M. B., Jan 2003. Dna damage activates atm through intermolecular autophosphorylation and dimer dissociation. Nature 421 (6922), 499–506.

Bar-Or, R. L., Maya, R., Segel, L. A., Alon, U., Levine, A. J., Oren, M., Oct 2000. Generation of oscillations by the p53-mdm2 feedback loop: a theoretical and experimental study. Proc Natl Acad Sci U S A 97 (21), 11250–11255.

Barak, Y., Juven, T., Haffner, R., Oren, M., Feb 1993. Mdm2 expression is induced by wild type p53 activity. EMBO J 12 (2), 461–468.

Barik, D., Paul, M. R., Baumann, W. T., Cao, Y., Tyson, J. J., Oct 2008. Stochastic simulation of enzyme-catalyzed reactions with disparate timescales. Biophys J 95 (8), 3563–3574.

Batchelor, E., Loewer, A., Lahav, G., May 2009. The ups and downs of p53: understanding protein dynamics in single cells. Nat Rev Cancer 9 (5), 371–377.

Batchelor, E., Mock, C. S., Bhan, I., Loewer, A., Lahav, G., May 2008. Recurrent initiation: a mechanism for triggering p53 pulses in response to dna damage. Mol Cell 30 (3), 277–289.

Bottani, S., Grammaticos, B., Nov 2007. Analysis of a minimal model for p53 oscillations. J Theor Biol 249 (2), 235–245.

Brooks, C. L., Gu, W., Feb 2006. p53 ubiquitination: Mdm2 and beyond. Mol Cell 21 (3), 307–315.

Cai, X., Yuan, Z.-M., Jul 2009. Stochastic modeling and simulation of the p53-mdm2/mdmx loop. J Comput Biol 16 (7), 917–933.

Chen, J., Lin, J., Levine, A. J., Jan 1995. Regulation of transcription functions of the p53 tumor suppressor by the mdm-2 oncogene. Mol Med 1 (2), 142–152.

Chène, P., May 2001. The role of tetramerization in p53 function. Oncogene 20 (21), 2611–2617.

Chickarmane, V., Nadim, A., Ray, A., Sauro, H. M., 2005. A p53 oscillator model of dna break repair control. Online.

Ciliberto, A., Capuani, F., Tyson, J. J., Mar 2007. Modeling networks of coupled enzymatic reactions using the total quasi-steady state approximation. PLoS Comput Biol 3 (3), e45.

Ciliberto, A., Novak, B., Tyson, J. J., Mar 2005. Steady states and oscillations in the p53/mdm2 network. Cell Cycle 4 (3), 488–493.

Dupont, G., Abou-Lovergne, A., Combettes, L., Sep 2008. Stochastic aspects of oscillatory ca2+ dynamics in hepatocytes. Biophys J 95 (5), 2193–2202.

Fang, S., Jensen, J. P., Ludwig, R. L., Vousden, K. H., Weissman, A. M., Mar 2000. Mdm2 is a ring finger-dependent ubiquitin protein ligase for itself and p53. J Biol Chem 275 (12), 8945–8951.

Feng, Z., Hu, W., de Stanchina, E., Teresky, A. K., Jin, S., Lowe, S., Levine, A. J., Apr 2007. The regulation of ampk beta1, tsc2, and pten expression by p53: stress, cell and tissue specificity, and the role of these gene products in modulating the igf-1-akt-mtor pathways. Cancer Res 67 (7), 3043–3053.

Freedman, D. A., Wu, L., Levine, A. J., Jan 1999. Functions of the mdm2 oncoprotein. Cell Mol Life Sci 55 (1), 96–107.

Gatz, S. A., Wiesmüller, L., Jun 2006. p53 in recombination and repair. Cell Death Differ 13 (6), 1003–1016.

Geva-Zatorsky, N., Rosenfeld, N., Itzkovitz, S., Milo, R., Sigal, A., Dekel, E., Yarnitzky, T., Liron, Y., Polak, P., Lahav, G., Alon, U., 2006. Oscillations and variability in the p53 system. Mol Syst Biol 2, 2006.0033.

Gibson, M. A., Bruck, J., Jul. 2001. Approximate accelerated stochastic simulation on chemically reacting systems. Journal of Chemical Physics 115 (4), 1716–1733.

Gillespie, D. T., 1977. Exact stochastic simulation of coupled chemical reactions. Journal of Physical Chemistry 81 (25), 2340–2361.

Goldbeter, A., Koshland, D. E., Nov 1981. An amplified sensitivity arising from covalent modification in biological systems. Proc Natl Acad Sci U S A 78 (11), 6840–6844.

Gonze, D., Halloy, J., Golberter, A., 2002a. Deterministic versus stochastic models for circadian rhythms. Journal of Biological Physics 28, 637–653.

Gonze, D., Halloy, J., Goldbeter, A., Jan 2002b. Robustness of circadian rhythms with respect to molecular noise. Proc Natl Acad Sci U S A 99 (2), 673–678.

Gottlieb, T. M., Leal, J. F. M., Seger, R., Taya, Y., Oren, M., Feb 2002. Cross-talk between akt, p53 and mdm2: possible implications for the regulation of apoptosis. Oncogene 21 (8), 1299–1303.

Goutsias, J., May 2005. Quasiequilibrium approximation of fast reaction kinetics in stochastic biochemical systems. J Chem Phys 122 (18), 184102.

Håkansson, P., Hofer, A., Thelander, L., Mar 2006. Regulation of mammalian ribonucleotide reduction and dntp pools after dna damage and in resting cells. J Biol Chem 281 (12), 7834–7841.

Hamstra, D. A., Bhojani, M. S., Griffin, L. B., Laxman, B., Ross, B. D., Rehemtulla, A., Aug 2006. Real-time evaluation of p53 oscillatory behavior in vivo using bioluminescent imaging. Cancer Res 66 (15),

7482–7489.

Hsu, Y.-L., Kuo, P.-L., Chiang, L.-C., Lin, C.-C., Sep 2004. Involvement of p53, nuclear factor kappab and fas/fas ligand in induction of apoptosis and cell cycle arrest by saikosaponin d in human hepatoma cell lines. Cancer Lett 213 (2), 213–221.

Hu, W., Feng, Z., Ma, L., Wagner, J., Rice, J. J., Stolovitzky, G., Levine, A. J., Mar 2007. A single nucleotide polymorphism in the mdm2 gene disrupts the oscillation of p53 and mdm2 levels in cells. Cancer Res 67 (6), 2757–2765.

Inoue, T., Geyer, R. K., Howard, D., Yu, Z. K., Maki, C. G., Nov 2001. Mdm2 can promote the ubiquitination, nuclear export, and degradation of p53 in the absence of direct binding. J Biol Chem 276 (48), 45255–45260.

Kruse, J.-P., Gu, W., May 2009. Modes of p53 regulation. Cell 137 (4), 609–622.

Kummer, U., Krajnc, B., Pahle, J., Green, A. K., Dixon, C. J., Marhl, M., Sep 2005. Transition from stochastic to deterministic behavior in calcium oscillations. Biophys J 89 (3), 1603–1611.

Lahav, G., 2008. Oscillations by the p53-mdm2 feedback loop. Adv Exp Med Biol 641, 28–38.

Lahav, G., Rosenfeld, N., Sigal, A., Geva-Zatorsky, N., Levine, A. J., Elowitz, M. B., Alon, U., Feb 2004. Dynamics of the p53-mdm2 feedback loop in individual cells. Nat Genet 36 (2), 147–150.

Lipniacki, T., Paszek, P., Brasier, A. R. A. R., Luxon, B., Kimmel, M., May 2004. Mathematical model of nf-kappab regulatory module. J Theor Biol 228 (2), 195–215.

Lozano, G., Elledge, S. J., Mar 2000. p53 sends nucleotides to repair dna. Nature 404 (6773), 24–25.

Ma, L., Wagner, J., Rice, J. J., Hu, W., Levine, A. J., Stolovitzky, G. A., Oct 2005. A plausible model for the digital response of p53 to dna damage. Proc Natl Acad Sci U S A 102 (40), 14266–14271.

Macnamara, S., Bersani, A. M., Burrage, K., Sidje, R. B., Sep 2008. Stochastic chemical kinetics and the total quasi-steady-state assumption: application to the stochastic simulation algorithm and chemical master equation. J Chem Phys 129 (9), 095105.

Mayo, L. D., Donner, D. B., Sep 2001. A phosphatidylinositol 3-kinase/akt pathway promotes translocation of mdm2 from the cytoplasm to the nucleus. Proc Natl Acad Sci U S A 98 (20), 11598–11603.

Mayo, L. D., Seo, Y. R., Jackson, M. W., Smith, M. L., Guzman, J. R., Korgaonkar, C. K., Donner, D. B., Jul 2005. Phosphorylation of human p53 at serine 46 determines promoter selection and whether apoptosis is attenuated or amplified. J Biol Chem 280 (28), 25953–25959.

McLure, K. G., Lee, P. W., Jun 1998. How p53 binds dna as a tetramer. EMBO J 17 (12), 3342–3350.

Offer, H., Wolkowicz, R., Matas, D., Blumenstein, S., Livneh, Z., Rotter, V., May 1999. Direct involvement of p53 in the base excision repair pathway of the dna repair machinery. FEBS Lett 450 (3), 197–204.

Oliner, J. D., Pietenpol, J. A., Thiagalingam, S., Gyuris, J., Kinzler, K. W., Vogelstein, B., Apr 1993. Oncoprotein mdm2 conceals the activation domain of tumour suppressor p53. Nature 362 (6423), 857–860.

Oren, M., Apr 2003. Decision making by p53: life, death and cancer. Cell Death Differ 10 (4), 431–442.

Oren, M., Maltzman, W., Levine, A. J., Feb 1981. Post-translational regulation of the 54k cellular tumor antigen in normal and transformed cells. Mol Cell Biol 1 (2), 101–110.

Pahl, H. L., Baeuerle, P. A., 1996. Control of gene expression by proteolysis. Current Opinion in Cell Biology 8, 340–347.

Proctor, C. J., Gray, D. A., 2008. Explaining oscillations and variability in the p53-mdm2 system. BMC Syst Biol 2, 75.

Puszyński, K., Hat, B., Lipniacki, T., Sep 2008. Oscillations and bistability in the stochastic model of p53 regulation. J Theor Biol 254 (2), 452–465.

Ramalingam, S., Honkanen, P., Young, L., Shimura, T., Austin, J., Steeg, P. S., Nishizuka, S., Jul 2007. Quantitative assessment of the p53-mdm2 feedback loop using protein lysate microarrays. Cancer Res 67 (13), 6247–6252.

Rao, C. V., Arkin, A. P., 2003. Stochastic chemical kinetics and the quasi-steady-state assumption: Application to the gillespie algorithm. Journal of Chemical Physics 118 (11), 4999–5010.

Reich, N. C., Oren, M., Levine, A. J., Dec 1983. Two distinct mechanisms regulate the levels of a cellular tumor antigen, p53. Mol Cell Biol 3 (12), 2143–2150.

Singh, B., Reddy, P. G., Goberdhan, A., Walsh, C., Dao, S., Ngai, I., Chou, T. C., O-Charoenrat, P., Levine, A. J., Rao, P. H., Stoffel, A., Apr 2002. p53 regulates cell survival by inhibiting pik3ca in squamous cell carcinomas. Genes Dev 16 (8), 984–993.

Stambolic, V., MacPherson, D., Sas, D., Lin, Y., Snow, B., Jang, Y., Benchimol, S., Mak, T. W., Aug 2001. Regulation of pten transcription by p53. Mol Cell 8 (2), 317–325.

Stommel, J. M., Wahl, G. M., Mar 2005. A new twist in the feedback loop: stress-activated mdm2 destabilization is required for p53 activation. Cell Cycle 4 (3), 411–417.

Toettcher, J. E., Loewer, A., Ostheimer, G. J., Yaffe, M. B., Tidor, B., Lahav, G., Jan 2009. Distinct mechanisms act in concert to mediate cell cycle arrest. Proc Natl Acad Sci U S A 106 (3), 785–790.

Tyson, J. J., 2006. Another turn for p53. Mol Syst Biol 2, 2006.0032.

Ventura, A., Kirsch, D. G., McLaughlin, M. E., Tuveson, D. A., Grimm, J., Lintault, L., Newman, J., Reczek, E. E., Weissleder, R., Jacks, T., Feb 2007. Restoration of p53 function leads to tumour regression in vivo. Nature 445 (7128), 661–665.

Vogelstein, B., Lane, D., Levine, A. J., Nov 2000. Surfing the p53 network. Nature 408 (6810), 307–310.

Vousden, K. H., Lane, D. P., Apr 2007. p53 in health and disease. Nat Rev Mol Cell Biol 8 (4), 275–283.

Wagner, J., Ma, L., Rice, J. J., Hu, W., Levine, A. J., Stolovitzky, G. A., Sep 2005. p53-mdm2 loop controlled by a balance of its feedback strength and effective dampening using atm and delayed feedback. Syst Biol (Stevenage) 152 (3), 109–118.

Wee, K. B., Surana, U., Aguda, B. D., 2009. Oscillations of the p53-akt network: implications on cell survival and death. PLoS ONE 4 (2), e4407.

Weinberg, R. L., Freund, S. M. V., Veprintsev, D. B., Bycroft, M., Fersht, A. R., Sep 2004. Regulation of dna binding of p53 by its c-terminal domain. J Mol Biol 342 (3), 801–811.

Zhang, T., Brazhnik, P., Tyson, J. J., Jan 2007. Exploring mechanisms of the dna-damage response: p53 pulses and their possible relevance to apoptosis. Cell Cycle 6 (1), 85–94.

Zhang, X.-P., Liu, F., Cheng, Z., Wang, W., Jul 2009. Cell fate decision mediated by p53 pulses. Proc Natl Acad Sci U S A 106 (30), 12245–12250.

Zhou, B. P., Liao, Y., Xia, W., Zou, Y., Spohn, B., Hung, M. C., Nov 2001. Her-2/neu induces p53 ubiquitination via akt-mediated mdm2 phosphorylation. Nat Cell Biol 3 (11), 973–982.

Legends

Figure 1: Schematic representation of the model. $\mathrm{Mdm2_{cyt}}$ and $\mathrm{Mdm2_{nuc}}$ denote cytoplasmic and nuclear Mdm2, respectively. $\mathrm{DNA_{dam}}$ stands for DNA damage. Normal arrows correspond to positive interactions, blunt arrows to negative interactions. Nuclear Mdm2 down regulates the level of p53 and is itself up regulated by nuclear translocation of cytoplasmic Mdm2. p53 exerts a positive control on the level of cytoplasmic Mdm2 (transcriptional activation) and a negative control on the level of nuclear Mdm2 (blockage of Mdm2 nuclear entry). DNA damage is induced by stress and exerts a negative control on the level of nuclear Mdm2, while p53 promotes damage repair.

Figure 2: Bifurcation diagrams and corresponding mean levels and oscillation periods for three different values of K_{Mc} and $K_{Mn} = 0.1$ nM. "sss" and "uss" refer to stable and unstable steady states, "slc" and "ulc" to stable and unstable limit cycles. $\mathrm{HB_{sc}}$ and $\mathrm{HB_{sb}}$ indicate supercritical and subcritical Hopf bifurcations; SNL : saddle-node loop.

Figure 3: Stochastic simulation for $K_{Mc} = 0.15$ nM and a damage repair rate $k_{Dam} = 0.02$ $\mathrm{h^{-1}}$. The basal value of d_{Mn} is 0.5 $\mathrm{h^{-1}}$. An irradiation dose IR = 30 (a.u.) is applied at time $t = 10$ h. **A**: Time evolution of p53, nuclear Mdm2 and damage levels for one run representing one cell. **B**: Distribution of the oscillation period in a population of 100 cells. CV is the coefficient of variation (std/mean).

Figure 4: Stochastic simulations for $K_{Mc} = 1.3$ nM and a damage repair rate $k_{Dam} = 0.02$ $\mathrm{h^{-1}}$. The basal value of d_{Mn} is 0.5 $\mathrm{h^{-1}}$. An irradiation dose IR = 7.8 (a.u.) is applied at time $t = 10$ h. **A**: Time evolution of p53, nuclear Mdm2 and damage levels for two runs corresponding to two different cells. *(left)*: Oscillations stop when damage is repaired. *(right)*: Oscillations continue temporarily after damage repair. **B**: Distribution of the oscillation period in a population of 100 cells. CV is the coefficient of variation (std/mean).

Figure 5: Stochastic simulations corresponding to individual cells for $K_{Mc} = 0.6$ nM and different repair rates. The basal value of d_{Mn} is 0.5 h^{-1}. **A**: High irradiation dose IR = 13 (a.u.) and low repair rate $k_{Dam} = 0.02$ h^{-1}. Region I: small amplitude oscillations with a characteristic period of $\sim$ 4.5 h. Region II: oscillations in the bi-cyclic domain. Region III: large amplitude oscillations with a period of $\sim$ 8.6 h. **B**: A high irradiation dose IR = 13 (a.u.) and a higher repair rate $k_{Dam} = 0.06$ h^{-1} lead to large amplitude oscillations. **C**: Large amplitude oscillations for a low irradiation dose IR = 5 (a.u.) and repair rate $k_{Dam} = 0.02$ h^{-1}.

Figure 6: The fraction of cells oscillating with high frequencies increases with the irradiation level. **A**: Simulations. Histograms of the characteristic period of p53 oscillations over the first 72 h after irradiation, for different irradiation doses. $K_{Mc} = 0.6$ nM, $k_{Dam} = 0.02$ h^{-1}. **B**: Experimental data from (Geva-Zatorsky et al., 2006, Figure 3). Histograms of the characteristic period of Mdm2-YFP signals (from 72 h movies) in MCF-7 cells exposed to different gamma irradiation doses 0, 0.3, 5, 10 Gy and for all cells. Reprinted by permission from Macmillan Publishers Ltd: Molecular Systems Biology, advance online publication, 2006 (doi: 10.1038/msb4100068).

Figure 7: Simulations of different oscillatory regimes at constant d_{Mn} values (no damage repair) and $\Omega = 1$. **A**: Large amplitude limit cycle for $K_{Mc} = 0.15$ nM, $d_{Mn} = 2$ h^{-1}. **B**: Small amplitude limit cycle for $K_{Mc} = 1.3$ nM, $d_{Mn} = 1.2$ h^{-1}. **C**: Simulation corresponding to the bi-cyclic domain for $K_{Mc} = 0.6$ nM, $d_{Mn} = 1.2$ h^{-1}. For each panel: *top* – stochastic dynamics of p53 for one run; *middle* – corresponding autocorrelation function (*black solid line*), and exponential fit (*red dashed line*); *bottom* – distributions of the individual peak amplitude and width divided by the mean value in a population of 100 cells. CV is the coefficient of variation.

Figure 8: Noise-induced pulses of p53 in individual cells for $K_{Mc} = 0.6$ nM. **A**: Sustained noise-induced oscillations around the stable node-focus at high damage (d_{Mn}=1.5 h^{-1}); characteristic period $\sim$ 5.3 h. **B**: Irregular p53 pulses induced by stochastic resonance in the multistationarity region at low d_{Mn} (d_{Mn}=0.6 h^{-1}).

Figure A1: Bifurcation diagrams and corresponding oscillation periods for three different values of K_{Mc} and $K_{Mn} = 0.3$ nM, a = 1 nM, $J_1 = J_2 = 0.1$ nM, $d_P = 0.6$ h^{-1}, $d'_P = 30$ h^{-1}. The other parameter values are as defined in Table 1 of the main text. "sss" and "uss" refer to stable and unstable steady states, "slc" and "ulc" refer to stable and unstable limit cycles. HB_{sc} and HB_{sb} indicate supercritical and subcritical Hopf bifurcations; SNL : saddle-node loop.

Table 1: Parameter values used for the differential equations (1) as well as for the Gillespie simulations. The cytoplasmic volume (V_c) is based on the volume of fibroblast cells : $\sim 2 - 3.4 \times 10^{-12}$ liter (Lipniacki et al., 2004; Håkansson et al., 2006). V_r is the cytoplasmic to nuclear volume ratio. The other parameters are based on the literature (Ma et al., 2005; Pahl and Baeuerle, 1996).

Table 2: Reaction channels corresponding to differential model (1). M_n, M_c and P are the numbers of molecules of nuclear Mdm2, cytoplasmic Mdm2 and p53, respectively; brackets refer to their corresponding concentration levels. Dam represents the number of damage units. w_i is the propensity of reaction R_i. V_c (resp. V_n) is the cytoplasmic (resp. nuclear) volume of the cell. $\mathcal{N}_A$ is the number of Avogadro, Ω is a scaling parameter that determines the number of molecules of each component in the system. Steps R_1 and R_2 represent the basal and Mdm2-mediated degradation of p53, respectively. Step R_3 refers to the production of p53 while step R_4 corresponds to the basal and p53-dependent production of cytoplasmic Mdm2. Step R_5 represents the degradation of cytoplasmic Mdm2. Steps R_6 and R_7 relate to the nuclear import of cytoplasmic Mdm2 (inhibited by p53) and nuclear export of nuclear Mdm2. R_8 corresponds to the degradation of nuclear Mdm2, which is accelerated by damage. Finally, step R_9 accounts for the induction of DNA damage by irradiation and R_{10} for the repair of damage mediated by p53.

Table 3: Average variability of p53 and nuclear Mdm2 peak amplitude and width at constant d_{Mn} values (without damage repair) for $\Omega = 1$. Estimations are done over 72 h of oscillations. Transient peaks in the first hours after damage induction are not considered. **Column 1**: variability of noise-induced oscillations in the multistationarity domain for $K_{Mc} = 0.6$ nM, $d_{Mn} = 0.6,\ 0.65\ \text{h}^{-1}$. **Column 2**: variability of large amplitude oscillations ($K_{Mc} = 0.15$ nM, $d_{Mn} = 1.5,\ 2.0\ \text{h}^{-1}$ and $K_{Mc} = 0.6$ nM, $d_{Mn} = 0.9,\ 1.0\ \text{h}^{-1}$). **Column 3**: variability in the bi-cyclic domain ($K_{Mc} = 0.6$ nM, $d_{Mn} = 1.2\ \text{h}^{-1}$). **Column 4**: variability of small amplitudes oscillations ($K_{Mc} = 1.3$ nM, $d_{Mn} = 1.0,\ 1.2\ \text{h}^{-1}$). **Column 5**: variability of noise-induced oscillations in the region of the stable node-focus ($K_{Mc} = 0.6$ nM, $d_{Mn} = 1.5,\ 1.6\ \text{h}^{-1}$). See supplementary material for detailed data.

Table 4: Average variability of p53 and nuclear Mdm2 peak amplitude and width with stochastic damage repair for $\Omega = 1$. Estimations are done over 72 h of oscillations. Transient peaks in the first hours after damage induction are not considered. **Column 1**: variability of large amplitude oscillations ($K_{Mc} = 0.15$ nM, $d_{Mn} = 1.5,\ 2.0\ \mathrm{h}^{-1}$ and $K_{Mc} = 0.6$ nM, $d_{Mn} = 0.9,\ 1.0\ \mathrm{h}^{-1}$). **Column 2**: variability of small amplitudes oscillations ($K_{Mc} = 1.3$ nM, $d_{Mn} = 1.0,\ 1.2\ \mathrm{h}^{-1}$). In each case, cells are stressed with irradiation doses that shift d_{Mn} from its basal value to the different values indicated above. Damage is then repaired with a rate $k_{Dam} = 0.02\ \mathrm{h}^{-1}$. See supplementary material for detailed data.

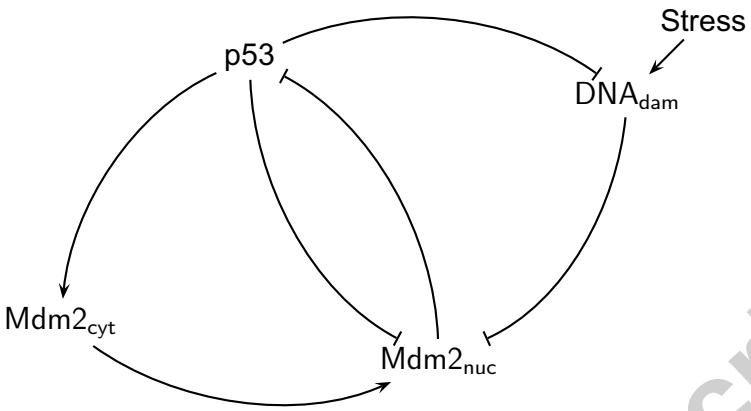

a

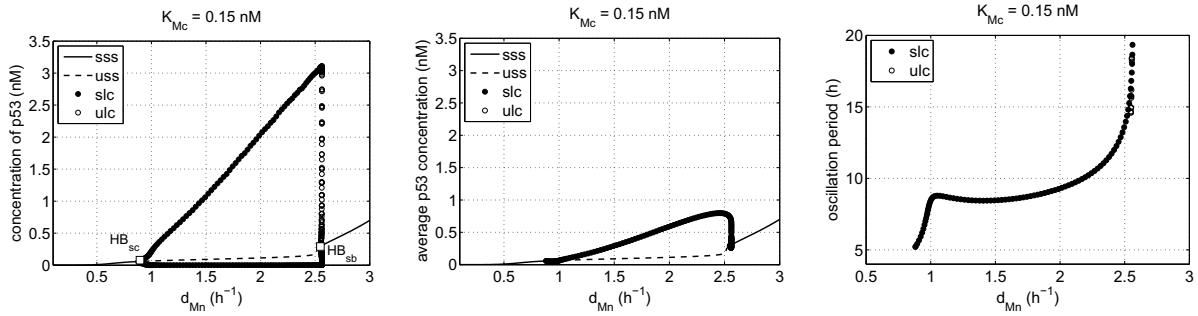

b

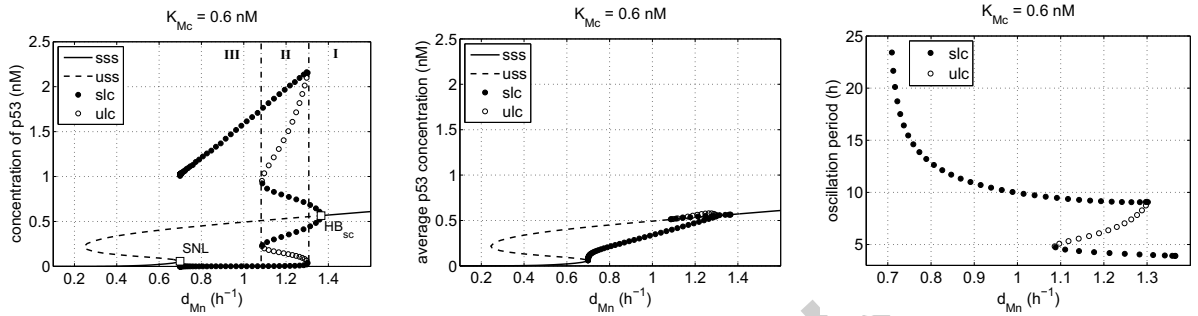

c

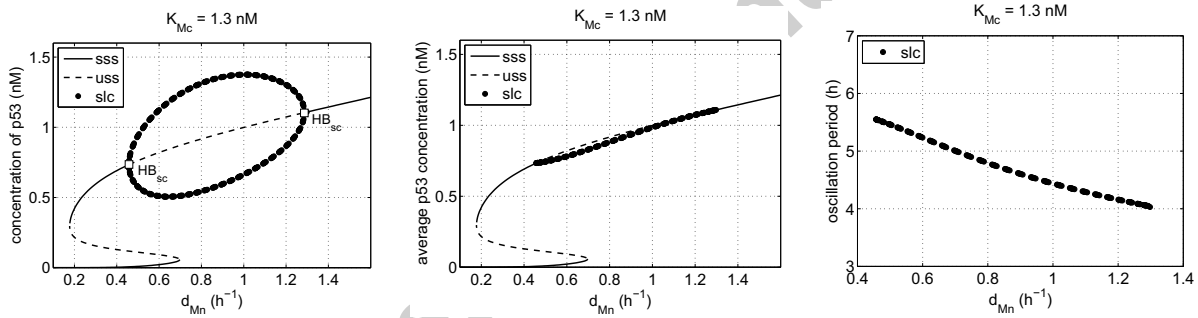

a

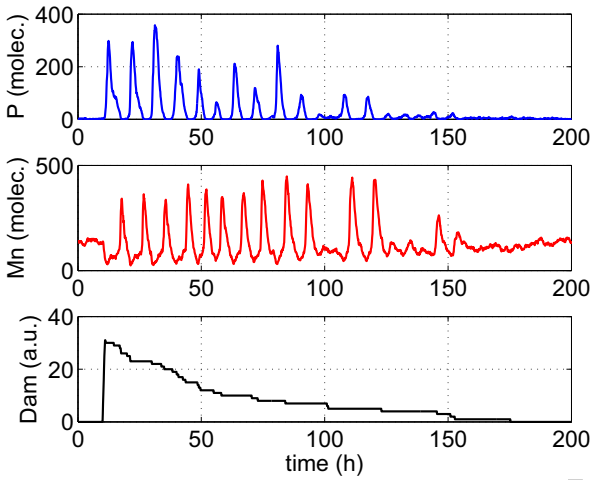

b

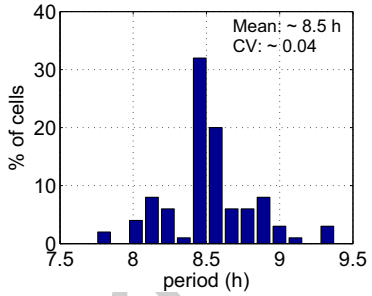

a

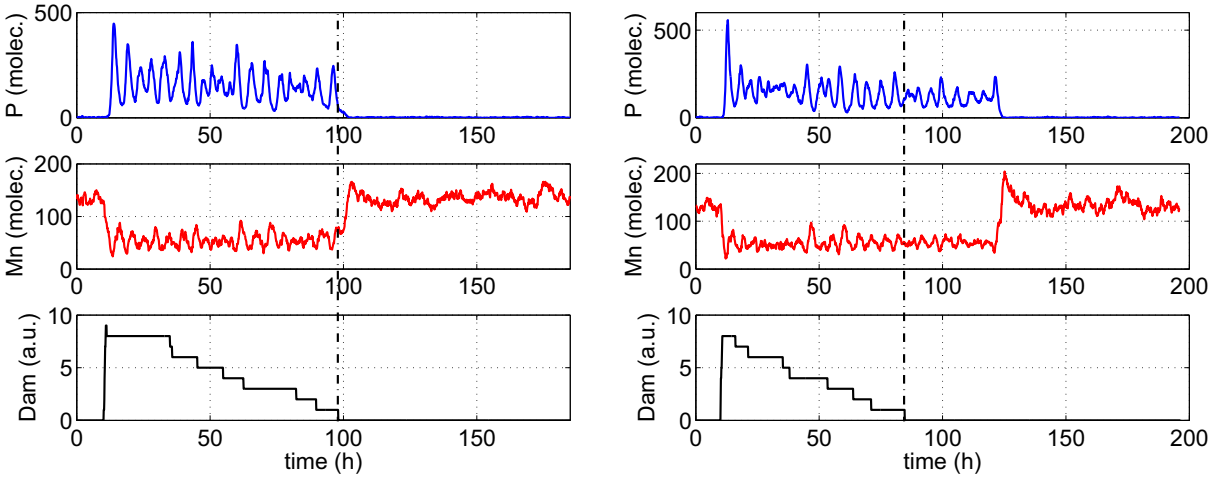

b

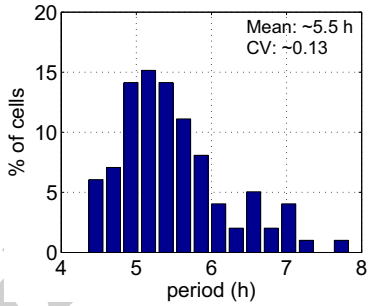

a

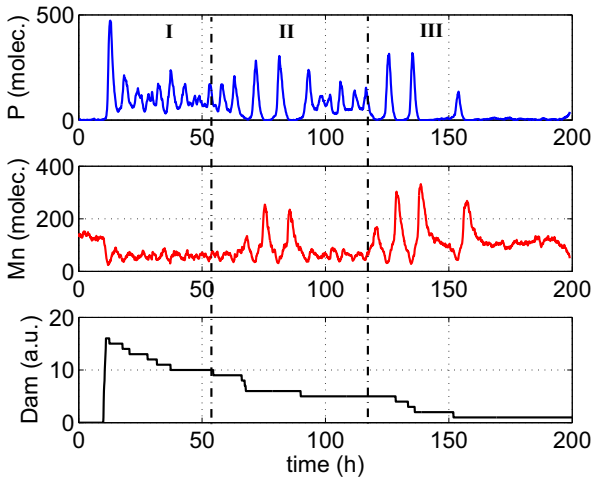

b

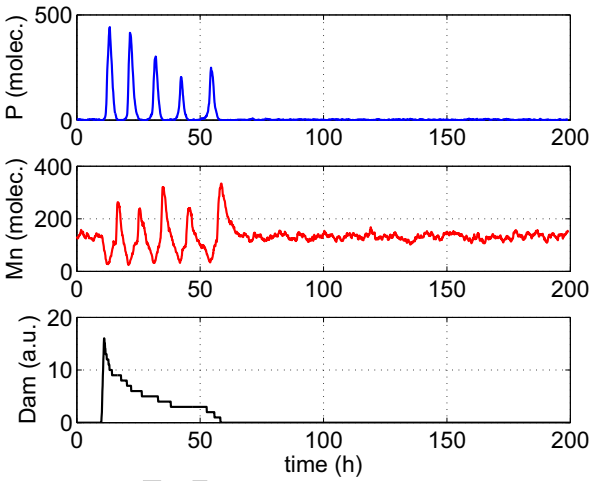

c

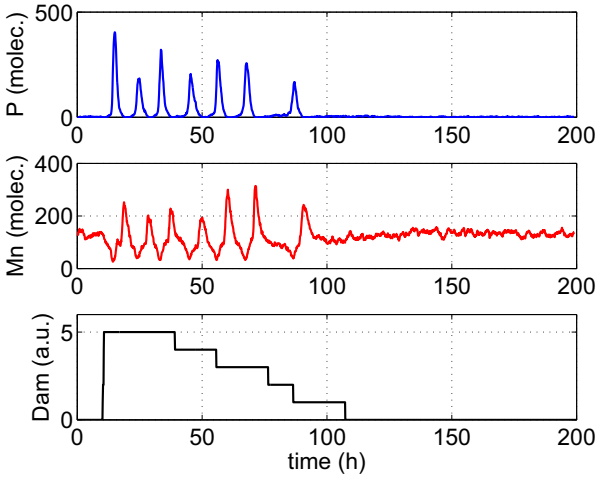

a

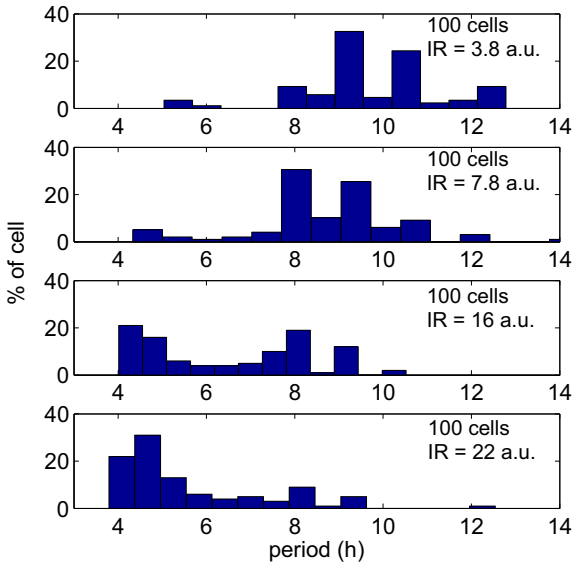

b

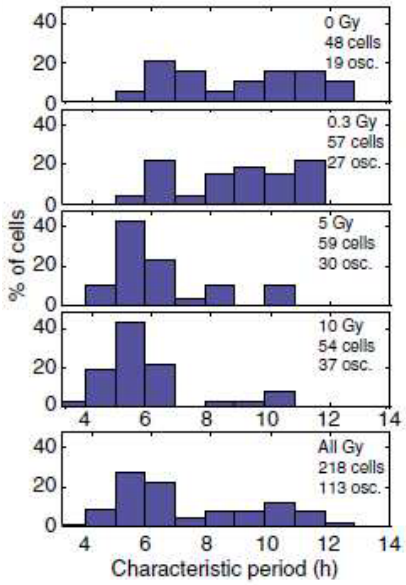

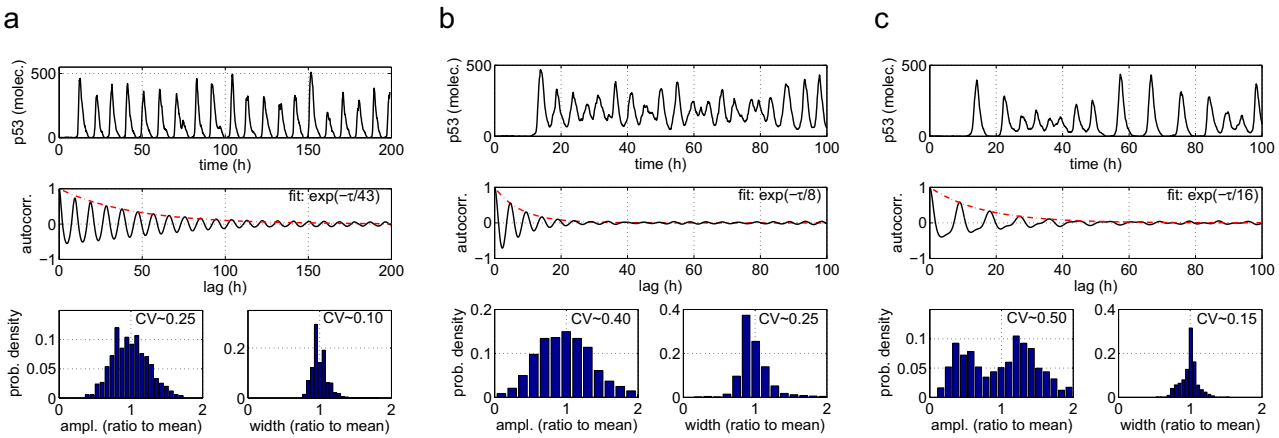

a

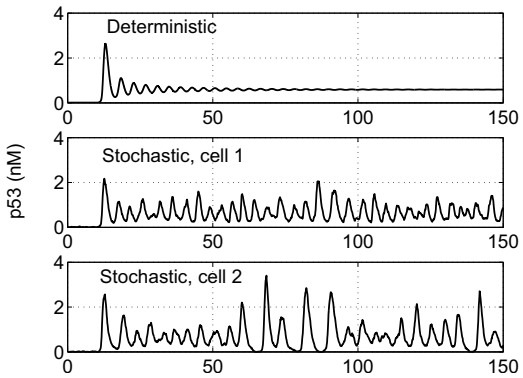

b

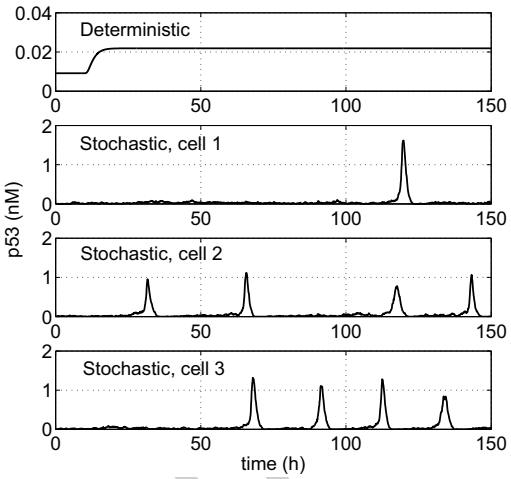

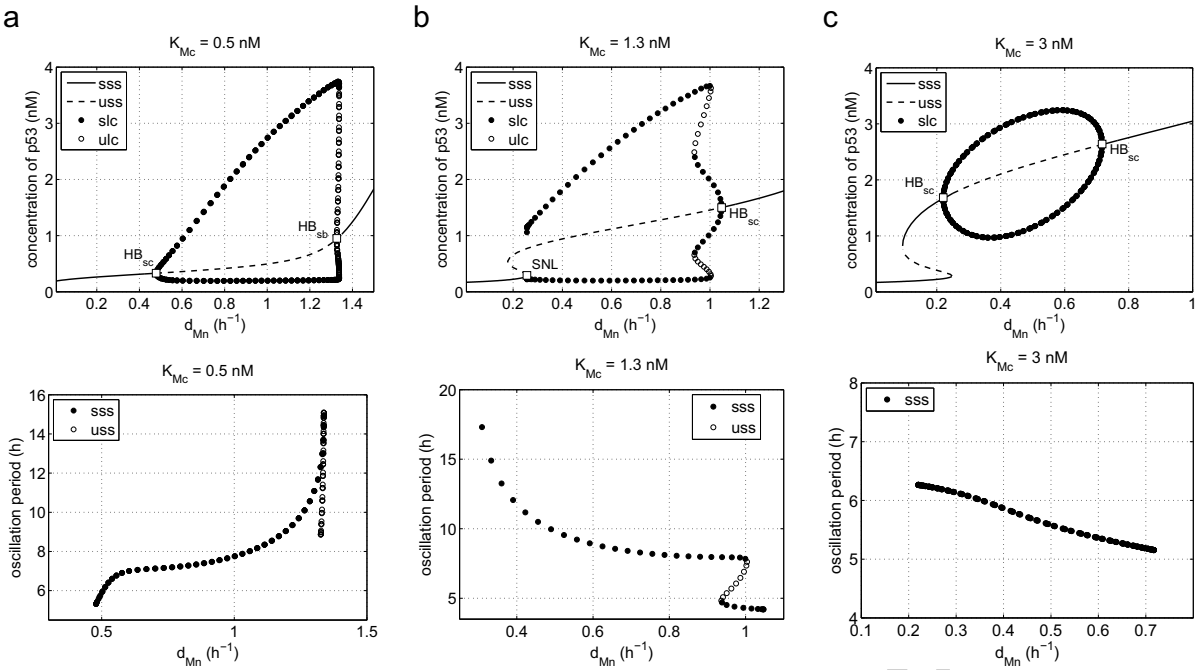

Protein production
$k_P = 5\,\mathrm{nM\,h^{-1}}$, $k_{Mc} = 0.1\,\mathrm{nM\,h^{-1}}$, $k'_{Mc} = 1.2\,\mathrm{nM\,h^{-1}}$
Protein degradation
$d_P = 0.1\,\mathrm{h^{-1}}$, $d'_P = 2.3\,\mathrm{nM^{-1}\,h^{-1}}$, $d_{Mc} = 0.6\,\mathrm{h^{-1}}$,
$d'_{Mn} = 0.5\,\mathrm{h^{-1}}$, $d''_{Mn} = 2.5\,\mathrm{h^{-1}}$
Translocation of Mdm2
$k_{in} = 0.45\,\mathrm{h^{-1}}$, $k'_{in} = 0.4\,\mathrm{h^{-1}}$, $k_{out} = 0.045\,\mathrm{h^{-1}}$
Dissociation and threshold constants
$K_P = 0.2\,\mathrm{nM}$, $K_{Mn} = 0.1\,\mathrm{nM}$, $K_{Mc} = 0.6\,\mathrm{nM}$,
$K_{Dam} = 0.001\,\mathrm{nM}$, $K'_{Mn} = 20$ Damage units
Other parameters
$k_{\mathrm{IR}} = 1$ Damage unit/IR dose, $k_{Dam} = 0.02\,\mathrm{h^{-1}}$,
$V_c = 2.7 \times 10^{-12}$ l, $V_r = 10$, $\Omega = 1$.

Reaction number i	Reaction step R_i	Reaction propensity w_i
1	$P \longrightarrow \star$	$w_1 = d_P P$
2	$P + Mn \longrightarrow Mn$	$w_2 = \frac{d'_p}{\Omega V_n \mathcal{N}_A} P\, Mn$
3	$\star \longrightarrow P$	$w_3 = \Omega V_n \mathcal{N}_A k_p \frac{(\Omega K_p)^4}{(\Omega K_p)^4 + [Mn]^4}$
4	$\star \longrightarrow Mc$	$w_4 = \Omega V_c \mathcal{N}_A \left(k_{Mc} + k'_{Mc} \frac{[P]^4}{(\Omega K_{Mc})^4 + [P]^4} \right)$
5	$Mc \longrightarrow \star$	$w_5 = d_{Mc} Mc$
6	$Mc \longrightarrow Mn$	$w_6 = \left(k_{in} - k'_{in} \frac{[P]^4}{(\Omega K_{Mn})^4 + [P]^4} \right) Mc$
7	$Mn \longrightarrow Mc$	$w_7 = k_{out} Mn$
8	$Mn \longrightarrow \star$	$w_8 = d_{Mn} Mn$, with $d_{Mn} = d'_{Mn} + d''_{Mn} \frac{Dam}{(K'_{Mn} + Dam)}$
9	$\mathrm{IR} \longrightarrow Dam$	$w_9 = k_{\mathrm{IR}} \mathrm{IR}$
10	$Dam \longrightarrow \star$	$w_{10} = k_{Dam} \frac{[P]^4}{(\Omega K_{Dam})^4 + [P]^4} Dam$

Variability of	Noise-induced oscillations (1)	Large amplitude	Bi-cyclic domain	Small amplitude	Noise-induced oscillations (2)
p53 ampl.	25%	30%	50%	40%	65%
p53 width	10%	10%	20%	25%	30%
nuc. Mdm2 ampl.	22%	20%	55%	45%	60%
nuc. Mdm2 width	35%	10%	30%	30%	30%

Variability of	Large amplitude oscillations	Small amplitude oscillations
p53 ampl.	45%	40%
p53 width	10%	35%
nuc. Mdm2 ampl.	25%	75%
nuc. Mdm2 width	15%	50%